

www.acsami.org Research Article

Controlled Experiments and Optimized Theory of Absorption Spectra of Li Metal and Salts

Subhayan Roychoudhury, ^L Zengqing Zhuo, ^{Ruimin Qiao, Liwen Wan, Yufeng Liang, Feng Pan, Yi-de Chuang, Pavid Prendergast, and Wanli Yang*}



Cite This: ACS Appl. Mater. Interfaces 2021, 13, 45488-45495



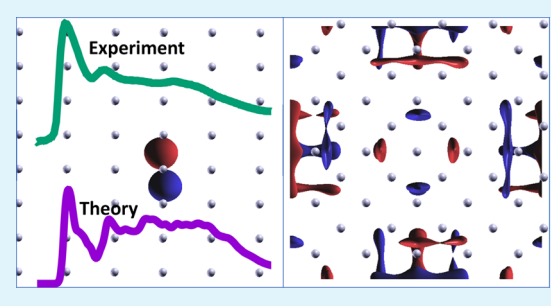
ACCESS

III Metrics & More

Article Recommendations

Supporting Information

ABSTRACT: Investigation of Li metal and ionic compounds through experimental and theoretical spectroscopy has been of tremendous interest due to their prospective applications in Li—metal and Li-ion batteries. Li K-edge soft X-ray absorption spectroscopy (sXAS) provides the most direct spectroscopic characterization; unfortunately, due to the low core-level energy and the highly reactive surface, Li—K sXAS of Li metal has been extremely challenging, as evidenced by many controversial reports. Here, through controlled and ultra-high energy resolution experiments of two kinds of *in situ* prepared samples, we report the intrinsic Li—K sXAS of Li—metal that displays a prominent leading peak that has not been revealed before.



Furthermore, theoretical simulations show that, due to the low number of valence electrons in Li, the Li–K sXAS is strongly affected by the response of the valence electrons to the core hole. We successfully reproduce the Li–K sXAS by state-of-the-art calculations with considerations of a number of relevant parameters such as temperature, energy resolution, and, especially, contributions from transitions which are forbidden in the single-particle treatment. Such a comparative experimental and theoretical investigation is further extended to a series of Li ionic compounds, which highlight the importance of considering the total and single-particle energies for obtaining an accurate alignment of the spectra. Our work provides the first reliable Li–K sXAS of the Li metal surface with advanced theoretical calculations. The experimental and theoretical results provide a critical benchmark for studying Li chemistry in both metallic and ionic states.

KEYWORDS: X-ray absorption spectroscopy, theory of spectroscopy, lithium metal, lithium salts, battery chemistry, Li-K spectroscopy

■ INTRODUCTION

Lithium-based batteries have been ubiquitous in modern life since their commercialization in the early 1990s. However, in spite of several decades of extensive efforts, the holy grail of a high-energy-density lithium battery based on a Li metal anode is yet to be achieved. The challenge of utilizing Li metal electrodes remains formidable in both practical optimization and fundamental understanding. Additionally, the electrolyte and its associated solid—electrolyte interphase and cathode—electrolyte interphase remain the least understood functional components, despite being critical to battery performance. Fundamentally, many limiting factors in battery operation are associated with Li-ion diffusion, which is extremely difficult to track due to the lack of techniques that could directly and precisely follow the lithium chemistry. Therefore, a direct probe of Li in its metallic and ionic states with elemental and chemical sensitivities becomes crucial.

The technical challenges for a direct probe of Li chemistry stem from many intrinsic characters. First, as an alkali metal, Li metal is highly reactive, so its surface is unstable under an ambient environment. As revealed by our controlled experiments below, even in an ultrahigh vacuum (UHV) environment, the chemical state of the surface of Li metal could still

evolve quickly in minutes, not to mention the typical Ar glovebox environment with a much higher level of reactive gas residuals. Second, as a popular technique, soft X-ray absorption spectroscopy (sXAS) has long been employed to study battery materials for many other elements, especially through its photon-in-photon-out (PIPO) mode with relative bulk sensitivity. However, the only core-level excitation of Li, the K-edge electron excitation from 1s to 2p, falls into a very low energy range, from 55 to 65 eV. This low energy naturally leads to a shallow probe depth (attenuation length ~50 nm, thus probe depth ~25 nm) even in the sXAS PIPO mode. Third, for ionic compounds, it has been observed that soft X-rays around the Li-K edge could introduce radiation damage effects.8 Therefore, experiments with controlled surface preparation and irradiation are both critical for obtaining reliable data. Fourth, due to these technical challenges,

Received: June 26, 2021 Published: September 16, 2021





compared with a large number of sXAS reports of other elements, for example, O and transition metals, there is only a handful of literature with experimental results of Li-K sXAS.⁸⁻¹⁶ Additionally, due to the lack of benchmark and fundamental understandings of Li-K spectra, Li-K sXAS, in spite of being the most direct spectroscopic probe of Li, was typically utilized as just a supplementary indication of the amount of Li during the lithiation/delithiation process. 16 Even worse, the reported spectra of Li metal have varied significantly between different reports, and all Li-K sXAS reports of Li metal contradict the findings by other techniques such as electron energy loss spectroscopy (EELS) and hard X-ray Raman spectroscopy (XRS). 9-11,17-19

Theoretically, Li-K sXAS of various ionic compounds has been computed^{20,21} with the help of Kohn–Sham (KS) density functional theory (DFT)^{22,23} and many-body perturbation theory. 24,25 Researchers also simulated Li-K sXAS of metallic Li using wave-function-based single-particle techniques and perturbative treatments. 19,26 However, the precision and validity of the theoretical calculations suffer from the lack of reliable experimental results, so it has been hard to achieve a quantitative level of comparison between the theory and experiment. Therefore, establishing a benchmark of reliable experimental data and developing theoretical calculations of Li-K are equally important toward the direct probe of Li chemistry through Li-K sXAS.

In this paper, controlled experiments were carried out by employing two kinds of in situ lithium-metal sample preparations, evaporation and cleaving, directly in UHV with ultrahigh experimental resolution (0.01 eV experimental resolution without core-hole lifetime considerations). Aging and radiation effects are tested separately. We show that the surface of Li metal is highly reactive, even in a 1.4×10^{-10} Torr UHV environment, evolving into a spectrally dominant Li₂O layer. Samples prepared by in situ Li evaporation in UHV display the degradation signature right after preparation, likely due to the immediate reaction at the high temperature of the evaporation process. Comparative experiments on three sets of samples show that the surface prepared through in situ cleaving finally rules out all degradation possibilities and allows the collection of the intrinsic Li-K spectrum of Li metal. Li-K sXAS of Li metal displays a prominent leading peak at the absorption edge that has never been found before in any Li-K techniques including sXAS, EELS, and XRS. Our theoretical calculations show that due to the low atomic number of Li, the poorly screened core hole strongly affects the unoccupied orbitals. An accurate calculation requires the explicit consideration of the orbital relaxation of all the valence electrons in response to the core hole creation, which we simulate with the many-body X-ray absorption spectroscopy (MBXAS) method.^{27–29} We successfully explore the effects of finite temperature, spectral resolution, and contributions from transitions which are forbidden within a simplified singleparticle framework, thereby achieving successful reproduction of the experimental data and explain the previous controversial reports. We further investigate a series of Li ionic compounds based on the same theoretical approach. The simulations show that accurate spectral alignment among different compounds can be obtained if each calculated spectrum is rigidly shifted by a term containing total energies as well as single-particle KS energies computed using a hybrid exact-exchange functional. Our work provides the first reliable data set of Li-K sXAS of Li metal through carefully controlled experiments, indicates the

possible sources of contradictions among the previous reports, and establishes the framework for optimized theoretical calculations to obtain a simulation of Li-K sXAS spectroscopy with quantitative accuracy in terms of spectral line shape and alignment.

EXPERIMENTAL AND THEORETICAL SECTION

Li-K sXAS was performed at the ultrahigh-energy-resolution Beamline 4.0.3 (MERLIN) of the Advanced Light Source at Lawrence Berkeley National Laboratory. The beamline covers energies ranging from 10 to ~150 eV, which is ideal for the Li K-edge, with a photon flux of $10^{11}/\text{sec}$. The experimental energy resolution is better than 10meV. Due to such a high instrumental resolution, it is expected that the finite peak width of the spectrum is predominantly a consequence of the thermal effects and the finite lifetimes of the Li quasiparticle orbitals, including the core hole and the conduction orbitals. Both total fluorescence yield (TFY) and the total electron yield (TEY) signals are collected; however, we note that due to the very low photon energy of Li-K around 50-60 eV, the attenuation of the Xray photons is around 50 nm (Supporting Information, Figure S5), so even for the TFY collected in the reflection-mode PIPO, the majority of the signals are from the surface \sim 20 nm, roughly at the same scale as the typical probe depth (\sim 5–10 nm) of TEY^{30,31} that is dominated by secondary electrons.³² This is confirmed by the similar Li-K TEY and TFY line shape of the Li-metal samples, as shown below. For Li salts, due to their highly insulating property, TEY suffers electrostatic charging upon irradiation, so we focus on TFY signals in this work.

Two different in situ sample preparation methods are used to prepare the Li metal samples: cleaving a thick piece of Li metal and Li evaporation. The in situ cleaving of the Li metal surface was done by installing a cleaned blade through a motion feedthrough into the UHV (1.4 \times 10⁻¹⁰ Torr) chamber, which is used to cut/scratch through the soft Li metal to expose a fresh surface. Evaporated Li metal surfaces are prepared by supplying a controlled current through a SAES Li metal dispenser, which has been well degassed before the Li evaporation. We note that SAES alkali metal dispensers are typical alkali metal sources in scientific studies for controlled alkali-metal evaporation in UHV.³³ Surprisingly, the two kinds of in situ prepared samples display clear spectral differences (Figures 1 and 2), which indicate the high reactivity of the Li metal surface even in 10⁻¹⁰ Torr UHV and provide the chance to clarify the discrepancies among previous reports.

On the theory front, we simulate the spectra with the MBXAS formalism which approximates the initial (final) state as a Slater determinant composed of two distinct sets of valence KS orbitals obtained in the absence (presence) of a core hole. As discussed in the next section, with such explicit consideration of the relaxation of valence electrons, MBXAS is able to show that electronic transitions which are forbidden in the conventional single-particle approach can actually have significant amplitude. For simulating room-temperature effects, we use MBXAS in conjunction with ab initio molecular dynamics (MD) which leads to an overall smoothening of the spectrum, in accordance with the experimental results. Finally, in order to obtain an accurate alignment among the spectra of different materials, we propose a scheme based on a combined consideration of the total and single-particle energies obtained using a nonlocal hybrid exact-exchange functional.

■ RESULTS AND DISCUSSION

Li-K Spectroscopy of Li Metal. Figure 1a shows the Kedge absorption spectra, collected in both the TFY and TEY modes, of Li metal samples immediately after the preparation through in situ cleaving (red) and in situ evaporation (blue). The in situ cleaved sample displays a striking leading peak. Such a dominating peak was not observed in previous Li-K sXAS reports at all, 10,11 and previous reports based on relatively bulk sensitive techniques found a much weaker

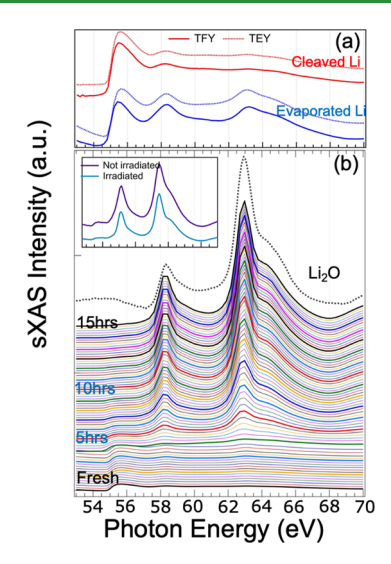


Figure 1. Soft X-ray Li–K sXAS collected on lithium metal surfaces prepared *in situ* in two different ways. (a) The red and the blue spectra show the Li K-edge of metallic Li prepared by *in situ* cleaving and evaporation, respectively. (b) Spectral evolution of a freshly cleaved Li metal surface (bottom spectrum) at every 10 min in UHV of 1.4×10^{-10} Torr. The 15 thick spectra indicate the line shape evolution every 1 h. Features from Li₂O emerge after only 20 min in UHV and dominate the degraded spectral line shape. The red spectrum in panel (a) is an amplified view of the bottom spectrum in panel (b). The inset shows spectra collected on two spots with and without X-ray exposure during the 5 h decay period in UHV. The line shape degrades in the same way with only small quantitative differences, indicating that the line shape decay is from surface aging and not irradiation effect.

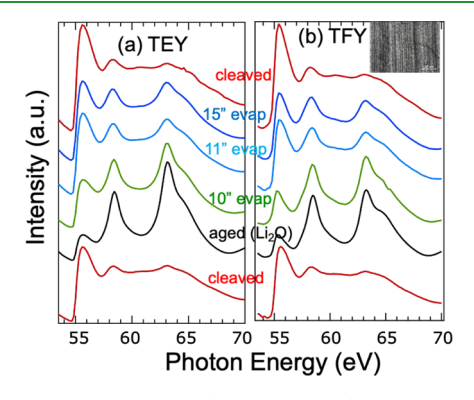


Figure 2. Li–K sXAS TEY (a) and TFY (b) spectra collected on lithium metal prepared in the sequence of (i) *in situ* cleaving (bottom, red), (ii) in-vacuum aged (black), (iii) lithium evaporation for 10 (green), 11 (light blue), and 15 (blue) minutes, and (iv) another *in situ* cleaving (top, red). Further lithium evaporation does not affect the overall spectral line shape above 11 min. However, the *in situ* cleaving is a robust method for highly reproducible Li–K sXAS data. The inset shows the optical image of a cleaved surface after bladescratching.

feature here. 11,17,26,34 This leading peak is also much suppressed in the evaporated Li spectra with enhanced features at high energies. As plotted in Figure 1b with the dashed line on top, these high-energy features match the Li₂O peaks, indicating that the sample surface already degraded right after the *in situ* evaporation of the Li metal.

To investigate the Li metal degradation even in UHV and to confirm that the spectra collected from the *in situ* cleaved Li metal are intrinsic Li metal signals, Figure 1b displays the sXAS

recorded right after the cleaved metal surface is exposed at a regular interval of 10 min each for 15 h. The bottommost spectrum is from the freshly prepared sample, the same as the spectrum amplified in Figure 1a. Moving from the bottom to the top, the 15 thick spectra indicate the line shape evolution every 1 h. Obvious change is observed after 20 min when the profound 55.6 eV feature begins to diminish and the features at 58.4 and 62.9 eV start intensifying. The latter two resemble the peaks of the Li₂O spectrum, as shown by the reference spectra on top. After about 4 h in the UHV chamber, evident features from Li₂O start to dominate the spectrum and the signatures of the freshly prepared Li sample are obscured. The results here clearly show that even at 10⁻¹⁰ Torr UHV, the Li metal surface still degrades quickly. This naturally explains why experiments with Li metal samples loaded from Ar bags, or even in air, reported very different results.^{9,10} Furthermore, the formation of Li₂O is intriguing because O₂ molecules are removed in the UHV environment, and residual gas molecules of UHV at 10⁻¹⁰ Torr scale are mostly water and others with light molecular weight. The dominating Li₂O signals as the degradation product of Li metal under UHV imply a multistep process instead of direct Li oxidation with O2 gas.

In order to rule out irradiation effects for such a spectral evolution, we collect the *in situ* spectrum of a separate sample, prepared and stored under similar conditions in the UHV for 5 h without any exposure to the X-ray beam. As shown in the inset of Figure 1b, this spectrum is essentially identical to that collected after 5 h from the sample which has been exposed to X-rays. This supports our inference that the disappearance of the 55.6 eV peak with time is due to surface degradation even under UHV and not due to irradiation.

To conclude our study of the intrinsic Li-K sXAS of Li metal, we further tested samples prepared in situ by both cleaving and evaporation on exactly the same piece of Li metal, as shown in Figure 2 with the sample preparation sequence from the bottom to the top. First, the cleaved Li metal sample displays a strong 55.6 eV leading peak, as found above. Second, the sample is left in UHV for about 3 h, which displays a clear signature of the degradation product of Li₂O. Third, we evaporate lithium onto the surface of the sample with the evaporation times of 10, 11, and 15 min. The intensity of the Li₂O features shows that the surface is getting cleaner with evaporation times up to 10 min, but further lithium evaporation longer than 11 min does not improve the overall spectral line shape. Fourth, the red spectrum on top was collected on the same sample but with the surface cleaved again with the blade.

Therefore, these three sets of controlled experiments consistently suggest that the Li metal surface is highly reactive even under UHV conditions, which has led to the disappearance of the strong leading peak in previous Li metal sXAS studies. Because *in situ* evaporation introduces a much higher local temperature around the sample, it is not surprising that a large amount of freshly evaporated Li degrades right after the deposition. Therefore, intrinsic Li metal K-edge sXAS could only be obtained within a short time after *in situ* cleaving of the sample under UHV conditions. More importantly, the *in situ* cleaved samples have displayed a very robust and reproducible strong 55.6 eV peak that has not been found before even with bulk-sensitive techniques. ^{18,19,26} It is thus critical to interpret and validate this as the intrinsic Li metal Li–K line shape and to understand the discrepancy

between the Li-K sXAS here and other K-edge spectroscopic

Theoretical Calculations of Li-K sXAS of Li Metal. In order to reproduce and understand the striking line shape of the intrinsic Li metal Li-K spectrum, we have explored different parameters and successfully developed the theoretical calculation of the Li K-edge sXAS based on DFT. Details of the computational parameters are presented in Supporting Information. The dipole transition matrix element for electronic excitation from an initial state $|\Psi_i\rangle$ to a final state $|\Psi_i\rangle$ is given by $\langle \Psi_i|\hat{O}|\Psi_i\rangle$, where \hat{O} is the many-electron dipole transition operator. In the single-particle initial-state approximation, one approximates this term by

$$\langle \Psi_{\rm f} | \hat{O} | \Psi_{\rm i} \rangle \approx S \langle \phi_{\rm c} | \hat{o} | \phi_{\rm core} \rangle$$
 (1)

where $\phi_{
m core}$ is the single-particle wave function of the core electron, ϕ_c is a KS-unoccupied (i.e., conduction band) orbital obtained with the initial (ground)-state DFT calculation in the absence of the core hole, \hat{o} is now the single-particle dipole transition operator, and S is a constant.

The simulation of the Li K-edge spectrum of the bulk Li metal using this treatment is presented at the bottom of Figure 3. The final-state full core hole (FCH) spectrum, where ϕ_c in

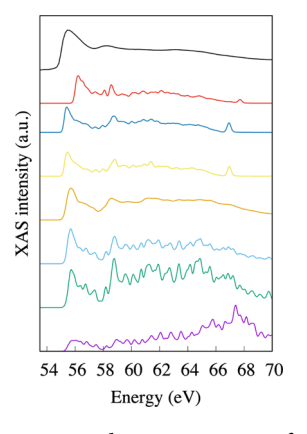


Figure 3. Plot showing X-ray absorption spectra of Li metal. From top to bottom: Experimental spectrum, simulated (with MBXAS) spectrum of the top layer of a 12-layer Li slab, spectrum of the fifth layer of the same slab, spectrum of the sixth layer of the slab, MBXAS spectrum of bulk Li crystal obtained from a MD snapshot sampled at 300 K temperature, MBXAS spectrum of the static bulk Li crystal, spectrum of bulk Li computed with the FCH treatment, spectrum of bulk Li simulated in the absence of the core hole. A broadening of 0.1 eV has been applied to all the simulated spectra.

eq 1 is replaced with $ilde{\phi}_{\scriptscriptstyle \mathcal{O}}$ a final-state conduction orbital evaluated in the presence of the core hole, is shown above it in the same figure. The stark difference between the initial-state and the FCH spectra stems from the fact that due to the low number of valence electrons in Li, the core hole is poorly screened, and consequently, the unoccupied orbitals obtained in the presence and absence of the core hole are very different. In fact, the presence of the core hole generates a set of localized orbitals trapped in the electrostatic potential of the excited core, which have significant overlap with the core orbital and result in higher-intensity transitions in the spectrum.

The blue spectrum labeled "MBXAS (bulk)" is obtained with the recently developed MBXAS method, which calculates the matrix element $\langle \Psi_f | \hat{O} | \Psi_i \rangle$ by approximating the many-body

wave function $\Psi_f(\Psi_i)$ by a Slater determinant composed of KS orbitals computed in the presence (absence) of the core hole. Unlike the FCH spectrum, the MBXAS spectrum replicates a key feature of the experimental plot: the intensity of the first narrow peak is higher than that of the broad region at higher energy. Many of the low-energy near-edge transitions, which have negligible probability in the single-particle treatment, have appreciable probability in the MBXAS treatment. Figure 4a,b shows the isovalue plots of two unoccupied KS orbitals,

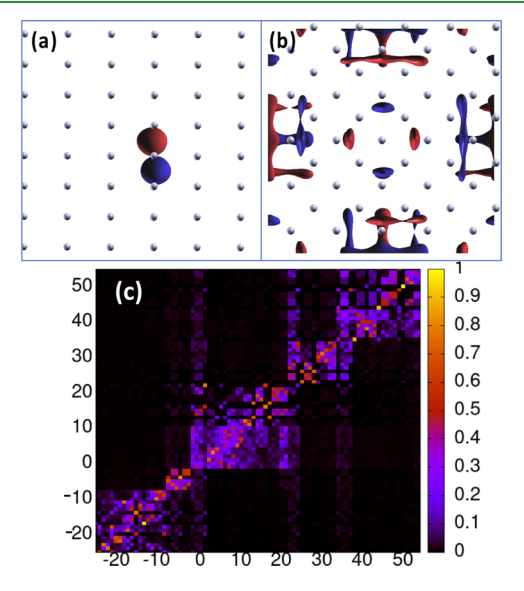


Figure 4. Panels (a,b) show the isovalue plots of two unoccupied final-state orbitals, transitions to which generate, according to the MBXAS treatment, two core excitations having appreciable probability and contributing to the high-intensity peak in the Limetal spectrum. Panel (a) shows a p-type orbital around the coreexcited atom, and consequently, such a transition is dominant in the FCH approach as well. However, the orbital in panel (b) shows no presence on the core-excited (central) atom and thus, the FCH calculation shows negligible probability for this transition. However, within the MBXAS treatment, both of the transitions correspond to appreciable probability. Panel (c) shows, within a certain range encompassing the highest occupied level, the absolute value of the overlap between the initial- and the final-state orbitals for the Γ point. The orbital with index = 1 is the lowest unoccupied level. As discussed in the main text (see the paragraph following eq 2), due to the presence of off-diagonal elements in this overlap matrix, it is possible that transitions which are forbidden in the single-particle FCH treatment have appreciable intensity in the MBXAS formalism.

transitions to which contribute significantly to the first peak intensity in MBXAS. While the orbital in panel (a) is a p-type orbital centered on the core-excited atom and is therefore representative of a standard dipole-allowed transition in the FCH treatment, the orbital in panel (b) has negligible spatial overlap with the core-excited atoms, and consequently, the associated single-particle excitation does not have any significant FCH transition probability. However, the latter excitation has a substantial probability in the MBXAS method, which computes the transition matrix element as

$$\langle \Psi_{f} | \hat{O} | \Psi_{i} \rangle = \sum_{c}^{empty} \langle \Psi_{f} | \Psi_{i}^{c} \rangle \langle \phi_{c} | \hat{o} | \phi_{core} \rangle$$
(2)

where $|\Psi_i^c\rangle$ represents an excited state (with the core orbital excited to the conduction orbital c) constructed with initialstate orbitals, which is represented by a Slater determinant composed of the valence-occupied initial-state KS orbitals along with ϕ_c . The term $\langle \Psi_f | \Psi_i^c \rangle$, a matrix element between two Slater determinants built from orbitals of different selfconsistent fields (final and initial state), can be re-expressed as the complex conjugate of a determinant composed of the overlap matrix elements between the final- and initial-state orbitals (see Supporting Information for more details). A heat map showing the absolute values of such orbital overlaps is shown in Figure 4c. The presence of significant off-diagonal elements in this overlap matrix indicates the possibility that even if, for a certain final-state orbital $\widetilde{\phi}_{c'}$, the transition probability $\langle \widetilde{\phi}_{c} | \hat{\delta} | \phi_{core} \rangle$ is zero (i.e., the transition is dipoleforbidden in the FCH picture), it is possible that for a finite number of unoccupied initial-state orbitals ϕ_c , both of the terms $\langle \phi_c | \hat{o} | \phi_{core} \rangle$ and $\langle \Psi_f | \Psi_i^c \rangle$ have nonzero contributions, leading to an appreciable transition probability given by the sum in eq 2 (note that $\Psi_{\rm f}$ is given by a Slater determinant, of which $\widetilde{\phi}_{\epsilon'}$ is a constituent orbital). The capability of including all these transition probabilities in our MBXAS calculations directly leads to the improved agreement with our experimental data on the strong 55.6 eV peak intensity beyond single-particle approximations.

In addition to the greater intensity of the first peak provided by the MBXAS theoretical approximation, we also note that there can be more mundane origins for a difference in relative intensity of the peaks. If, instead of a Gaussian broadening of 0.1 eV, we use a much higher broadening of 0.6 eV, the relative intensity of the higher-energy region of the MBXAS spectrum turns out to exceed that of the first peak (see Supporting Information). Therefore, in addition to surface aging reactions, a lower instrumental resolution can result in an experimental spectrum with a relatively lower first-peak intensity. This naturally explains the quantitative difference between the highresolution (10 meV experimental resolution) Li-K sXAS revealed here and the previous reports of hard XRS and EELS results. 18,19,25

In order to obtain a more realistic simulation of the experiment, which is performed at room temperature, we run a first-principles MD simulation on a 128-atom lithium crystal supercell at 300 K temperature and calculate, using the MBXAS method, the average sXAS spectrum on a sample snapshot (see previous examples in ref 20). The spectrum so obtained, which is labeled as "MD (bulk)" in Figure 3, can be seen to reproduce not only the prominent experimental peak at ~55.6 eV but also the less intense feature at ~58.5 eV. Comparing this with the "MBXAS(bulk)" spectrum obtained at zero temperature, we can see that the thermal motion of the ions is responsible for the relative smoothness of the former spectrum at higher energies. In order to check for possible effects of surface layers on the spectrum, we run MBXAS simulations on a 12-layer (18.85 Å) thick slab of Li atoms. In Figure 3, we have shown the computed spectra corresponding to the top layer, the fifth layer, and the sixth (middle) layer of the Li slab. MBXAS spectra for the fifth and the sixth layer of the slab look almost identical, indicating convergence. The spectra of these layers also replicate the crucial experimental observation that the narrow first peak has higher intensity than the high-energy region. It is worth noting that the top-layer spectrum blue-shifts to higher energies (~0.8 eV) due to the slightly lower electron population (i.e., oxidation) of the

surface, undercoordinated Li atoms. A lower ground-state valence Lowdin population (0.8524) on a surface atom compared to the one in the middle of the slab (0.9797) results in a higher binding energy for the core electron in the former. From Figures 3 and S3, we conclude that only the spectrum of the topmost undercoordinated layer bears any significant difference from the bulk spectrum and that, in terms of the position and intensity of the first peak, the bulk limit is attained to an appreciable extent from the second layer onward. A linear combination of the layer-by-layer spectra may lead to an intrinsic broadening of the first peak, evident in the bulk spectra, due to the relative prominence of this top-layer contribution. The representative KS orbitals corresponding to different regions of the simulated spectrum are shown in Figure S6.

Spectroscopy of Li-Based Ionic Compounds. Figure 5a shows the experimental spectra of a series of Li-based ionic

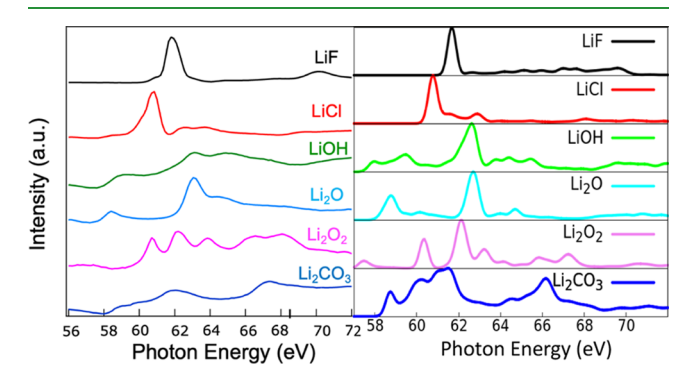


Figure 5. Panel (a) shows the experimental Li K-edge sXAS spectra of LiF, LiCl, LiOH, Li₂O, Li₂O₂, and Li₂CO₃. Panel (b) shows the theoretical counterparts simulated with MBXAS. A broadening of 0.2 eV has been applied to all of the simulated spectra. For discussion on the spectral alignment, see the main text.

compounds, which are of interest for being crucial components of the interphases in batteries as mentioned earlier, namely, LiF, LiCl, LiOH, Li₂O, Li₂O₂, and Li₂CO₃. The spectra for the latter three compounds, which were reported in our earlier work,8 exploring the effects of irradiation on Li K-edge spectroscopy, have been included here for the sake of completeness and comparison. It is clear that these Li ionic systems display very different line shapes with features at characteristic energy positions. Figure 5b shows the theoretical counterparts obtained with MBXAS calculations. Note that these spectra, which are simulated on the static crystal structure at zero temperature, do not incorporate the effects of thermal motion of the ions, which, in addition to smoothening the spectra further, may give rise to new spectral features as a result of local symmetry breaking. 20 For each of the compounds, in Figure S2, we present the isovalue plots of representative KS orbitals contributing to a prominent peak in the spectrum. In general, these orbital plots confirm that in keeping up with the ionic nature of the compounds, the bright peaks are associated mostly with unoccupied KS orbitals with large Li-p contribution. However, this trait is less pronounced in Li₂CO₃, where the contributing orbital shows noticeable delocalization, albeit with a significant Li-p character. Additionally, we also plot a KS orbital corresponding to the small prepeak below 58 eV in the Li₂O₂ spectrum. This KS level, which primarily displays oxygen orbital characters hybridized with some contribution from Li-p, can be associated with the

low-energy feature reported in the O K-edge RIXS study of Li₂O₂.35

sXAS Energy Alignment. In the same way that experimental measurements of sXAS require some calibration to align the spectral energies, the simulations performed in this work have their own alignment scheme. However, it is worth noting that the scheme adopted here, as in previous work, 20,36,37 relies only on a single experimental spectrum for calibration of all such spectra, defined by the element and the core orbital. Thereafter, all computed spectra should be predictive. This is particularly important when determining the contributions of multiple components to a given spectrum since their relative alignment can affect the final spectrum, for example, the different peak positions of the surface versus bulk Li atoms of Li metal as detailed above.

In our approach, we focus on the particular excited state that we model explicitly at the level of DFT self-consistent-field (SCF) calculations, which is the energetically lowest possible core-excited state for the given element and core orbital. This state has been referred to in the literature as the XCH state (excited electron and core hole),³⁸ referring to a neutral reference. XCH is different from the FCH (full core hole) state, which refers to the non-neutral (+1) ionization potential for the core electron. Using relative XCH total energies, we can align our calculated spectra. The energy ranges of the spectra themselves are defined by the corresponding KS eigenvalues from the XCH SCF, referenced to the highest occupied molecular orbital from the XCH calculation (which should have the same orbital index as the conduction band minimum or the lowest unoccupied molecular orbital of the ground state). Being familiar with expected underestimation ^{39,40} of both the electronic band gap and bandwidth by local and semilocal approximations to the exchange-correlation potential in DFT (such as PBE⁴¹), here we make use of the HSE hybrid exact-exchange functional.⁴² For insulators with large band gaps, HSE offers more accurate band structure estimates.

We elucidate the computational scheme with the example of LiF. The lowest possible core-excitation energy can be calculated as $(E_{\rm XCH} - E_{\rm GS})$, where $E_{\rm GS}$ $(E_{\rm XCH})$ corresponds to the total energy of the ground state (lowest core-excited state) calculation. However, since these two calculations employ different sets of pseudopotentials, their energies cannot be compared directly, and we resort to using a relative excitation energy by referencing the appropriate isolated atom

$$(E_{\rm XCH} - E_{\rm GS}) - (E_{\rm XCH}^{\rm atom} - E_{\rm GS}^{\rm atom})$$
 (3)

where E_{GS}^{atom} (E_{XCH}^{atom}) refers to the energy of a single Li atom in its ground state (lowest core-excited state) obtained with a charge-neutral DFT calculation employing the standard pseudopotential (pseudopotential containing a core hole). One can think of this relative excitation energy as equivalent to a formation energy difference.³⁶ In order to guarantee cancelation of systematic errors, the atomic calculations are performed within the same supercell as the full system with the same numerical parameters (plane-wave cutoff, k-point sampling, etc.).

The electronic structure of crystalline LiF exhibits a conduction band minimum with Li 2s symmetry. Unsurprisingly, the XCH state places the core-excited electron in a localized orbital with the Li 2s symmetry centered on the coreexcited Li atom. Therefore, the XCH state defines a dark exciton since $1s \rightarrow 2s$ transitions are dipole-forbidden. The

ground state has N valence electrons, and hence, the coreexcited states have N + 1 valence electrons. Therefore, the highest occupied molecular orbital of the XCH state has a KS eigenvalue $\tilde{\epsilon}_{N+1}$. Our calculations indicate that the first bright transition is to the orbital with energy $\tilde{\epsilon}_{N+3}$. Therefore, the position of the first bright transition in LiF could be approximated as

$$(E_{\text{XCH}} - E_{\text{GS}}) - (E_{\text{XCH}}^{\text{atom}} - E_{\text{GS}}^{\text{atom}}) + (\tilde{\varepsilon}_{N+3} - \tilde{\varepsilon}_{N+1})$$

$$+ E_{\text{shift}}$$
(4)

We apply an analogous expression to align the spectra of each excited atom in all the studied materials, where the orbital index of the first bright transition must be determined in each case. The constant, $E_{\text{shift}} = 56.6 \text{ eV}$, is added to each spectrum to align it with the experimental photon energy. It was deduced specifically to align the LiF first peak, and it depends on the specific pseudopotential approximations used (i.e., it is likely not directly transferrable to other calculations, which would require their own constant shift). All other energies in eq 4 are calculated using the HSE functional. However, the overall spectrum is still computed in its entirety using the PBE functional without any dilation factor because the necessary calculations of many unoccupied orbitals are currently too expensive using HSE. There is one exception to this rule: for the spectral alignment of Li metal using eq 4, the PBE functional is used exclusively since a local/semilocal functional is better suited for metallic systems in which the properties of the valence electrons are similar to that of the uniform electron gas.⁴⁴ Admittedly, this indicates some obvious room for improvement in finding an optimal and transferrable functional and is the subject of future research. As can be seen in Figure 5a,b, with some quantitative line shape differences, our calculated spectra show an excellent energy value in agreement with the features found in experimental data for all the Li salt compounds tested here.

CONCLUSIONS

In summary, we have presented a thorough and accurate account of experimental and theoretical investigation of Li Kedge sXAS of Li metal and salts. Our experimental findings indicate that due to the highly reactive Li metal surface, a reliable Li-K sXAS spectrum of Li metal could only be achieved on fresh in situ -cleaved samples in UHV. Additionally, theoretical calculations show that energy resolution will strongly affect the spectral intensity, especially for the first peak, leading to a modified line shape found in other bulk sensitive techniques compared with the ultra-high resolution Li-K sXAS here. These effects naturally explain the different Li-K line shapes of Li metal in previous controversial reports. We thus conclude that the intrinsic Li-K sXAS spectrum of Li metal features a striking peak at 55.6 eV with a high intensity.

This provides the opportunity to test different parameters and effects in theoretical calculations. We show that the popular FCH/XCH approach, which expresses the approximate transition probability in terms of the core and the conduction orbital only, is inadequate for reproducing the experimental features. The explicit, many-body response of all the valence electrons to the creation of the core hole must be taken into account, which we do by approximating the true wave function using a KS Slater determinant. Simulations based on room-temperature MD sampling show that thermal motion of the ions plays a crucial role in the smoothening of the spectral line shape. Eventually, we successfully reproduced the experimental results by considering these different effects and contributions from surface atoms, noting the appreciable contributions of nondipole single-particle transitions to the many-body transition amplitudes in our MBXAS calculations.

In addition to Li metal, we also extended our experimental and theoretical studies to a series of Li-based ionic compounds involved in energy storage materials. We further show the importance of considering total energies as well as KS eigenvalues obtained with hybrid functionals in order to obtain precise relative energy alignment of the spectra of different materials. This work provides a reliable data bank for Li–K spectroscopy of both Li metal and several important salts, as well as developments of theoretical calculations that could reproduce the experimental results at a quantitative level in both the line shape and energy alignment. The results set a solid benchmark for studying lithium chemistry through Li-K sXAS and reveal critical electronic parameters that define the chemistry of Li compounds.

ASSOCIATED CONTENT

5 Supporting Information

The Supporting Information is available free of charge at https://pubs.acs.org/doi/10.1021/acsami.1c11970.

Brief account of the determinant-based technique used in MBXAS, MBXAS plot of the Li K-edge of Li metal using two different values for broadening, isovalue plot of representative orbitals contributing to the different peaks in the absorption spectra of some of the Li-based compounds, contribution from different layers in MBXAS of a Li slab, plot showing standard deviation in the sXAS spectrum of all the Li atoms present in the MD snapshot, and plot of X-ray attenuation length as a function of photon energy (PDF)

AUTHOR INFORMATION

Corresponding Authors

Yi-de Chuang — Advanced Light Source, Lawrence Berkeley National Laboratory, Berkeley, California 94720, United States; ⊕ orcid.org/0000-0002-2773-3840;

Email: ychuang@lbl.gov

David Prendergast — The Molecular Foundry, Lawrence Berkeley National Laboratory, Berkeley, California 94720, United States; orcid.org/0000-0003-0598-1453; Email: dgprendergast@lbl.gov

Wanli Yang — Advanced Light Source, Lawrence Berkeley National Laboratory, Berkeley, California 94720, United States; orcid.org/0000-0003-0666-8063; Email: wlyang@lbl.gov

Authors

Subhayan Roychoudhury — Advanced Light Source and The Molecular Foundry, Lawrence Berkeley National Laboratory, Berkeley, California 94720, United States

Zengqing Zhuo — Advanced Light Source, Lawrence Berkeley National Laboratory, Berkeley, California 94720, United States; © orcid.org/0000-0001-6602-760X

Ruimin Qiao – Advanced Light Source, Lawrence Berkeley National Laboratory, Berkeley, California 94720, United States Liwen Wan − Lawrence Livermore National Laboratory, Livermore, California 94550, United States; orcid.org/ 0000-0002-5391-0804

Yufeng Liang — The Molecular Foundry, Lawrence Berkeley National Laboratory, Berkeley, California 94720, United States

Feng Pan — School of Advanced Materials, Peking University Shenzhen Graduate School, Shenzhen 518055, China; orcid.org/0000-0002-8216-1339

Complete contact information is available at: https://pubs.acs.org/10.1021/acsami.1c11970

Author Contributions

¹S.R., Z.Z. and R.Q. are contributed equally.

Notes

The authors declare no competing financial interest.

ACKNOWLEDGMENTS

The experiments were performed at BL4.0.3 of the Advanced Light Source (ALS), a DOE Office of Science User Facility at the Lawrence Berkeley National Laboratory (LBNL). Theory effort is supported by the LDRD Program at the LBNL and facilitated by a user program at The Molecular Foundry (TMF). Computational resources were provided by the Lawrencium and the TMF clusters (managed by the High Performance Computing Services Group, at LBNL) and by the National Energy Research Scientific Computing Center (NERSC). W.Y. acknowledges the support from the DOE Data, Artificial Intelligence, and Machine Learning at the DOE Scientific User Facilities project. All the facilities and efforts are supported by the Office of Science of the US DOE under contract no. DE-AC02- 05CH11231. We would like to thank Tod Pascal for helpful discussions and advice.

REFERENCES

- (1) Reddy, M. V.; Mauger, A.; Julien, C. M.; Paolella, A.; Zaghib, K. Brief History of Early Lithium-Battery Development. *Materials* **2020**, 13, 1884.
- (2) Lin, D. Reviving the Lithium Metal Anode for High-Energy Batteries. *Nat. Nanotechnol.* **2017**, *12*, 13.
- (3) Krauskopf, T.; Richter, F. H.; Zeier, W. G.; Janek, J. Physicochemical Concepts of the Lithium Metal Anode in Solid-State Batteries. *Chem. Rev.* **2020**, *120*, *7745*–*7794*.
- (4) Winter, M.; Barnett, B.; Xu, K. Before Li Ion Batteries. Chem. Rev. 2018, 118, 11433–11456.
- (5) Xu, K. Electrolytes and Interphases in Li-Ion Batteries and Beyond. Chem. Rev. 2014, 114, 11503-11618.
- (6) Lin, F.; Liu, Y.; Yu, X.; Cheng, L.; Singer, A.; Shpyrko, O. G.; Xin, H. L.; Tamura, N.; Tian, C.; Weng, T.-C.; Yang, X.-Q.; Meng, Y. S.; Nordlund, D.; Yang, W.; Doeff, M. M. Synchrotron X-Ray Analytical Techniques for Studying Materials Electrochemistry in Rechargeable Batteries. *Chem. Rev.* **2017**, *117*, 13123–13186.
- (7) Henke, B. L.; Gullikson, E. M.; Davis, J. C. X-Ray Interactions: Photoabsorption, Scattering, Transmission, and Reflection at E=50-30000 EV, Z=1-92. *Atomic Data Nucl. Data Tables* **1993**, *54*, 181–342.
- (8) Qiao, R.; Chuang, Y.-D.; Yan, S.; Yang, W. Soft X-Ray Irradiation Effects of Li2O2, Li2CO3 and Li2O Revealed by Absorption Spectroscopy. *PloS One* **2012**, *7*, No. e49182.
- (9) Braun, A.; Wang, H.; Shim, J.; Lee, S. S.; Cairns, E. J. Lithium K(1s) Synchrotron NEXAFS Spectra of Lithium-Ion Battery Cathode, Anode and Electrolyte Materials. *J. Power Sources* **2007**, *170*, 173–178.

- (10) Wang, D.; Zuin, L. Li K-Edge X-Ray Absorption near Edge Structure Spectra for a Library of Lithium Compounds Applied in Lithium Batteries. *J. Power Sources* **2017**, 337, 100–109.
- (11) Tsuji, J.; Nakamatsu, H.; Mukoyama, T.; Kojima, K.; Ikeda, S.; Taniguchi, K. Lithium K-Edge XANES Spectra for Lithium Compounds. *X-Ray Spectrom.* **2002**, *31*, 319–326.
- (12) Yogi, C.; Takamatsu, D.; Yamanaka, K.; Arai, H.; Uchimoto, Y.; Kojima, K.; Watanabe, I.; Ohta, T.; Ogumi, Z. Soft X-Ray Absorption Spectroscopic Studies with Different Probing Depths: Effect of an Electrolyte Additive on Electrode Surfaces. *J. Power Sources* **2014**, 248, 994–999.
- (13) Mizota, H.; Ito, Y.; Tochio, T.; Handa, K.; Takekawa, S.; Kitamura, K. Li K-Edge XANES Spectra of Lithium Niobate and Lithium Tantalite. *In AIP Conference Proceedings*; AIP: Stanford, California (USA), 2007; Vol. 882, pp 508–510.
- (14) O'Shaughnessy, C.; Henderson, G. S.; Moulton, B. J. A.; Zuin, L.; Neuville, D. R. A Li K -Edge XANES Study of Salts and Minerals. *J. Synchrotron Radiat.* **2018**, *25*, 543–551.
- (15) Orikasa, Y.; Furutani, J.; Yamanaka, K.; Ohta, T.. Lithium K-Edge X-Ray Absorption Analysis of Lithium-Ion Battery Cathodes. **2019**, No. *21*, 11. DOI: 10.34521/srmemoirs.21.0 11
- (16) Zhuo, Z.; Dai, K.; Qiao, R.; Wang, R.; Wu, J.; Liu, Y.; Peng, J.; Chen, L.; Chuang, Y.-d.; Pan, F.; Shen, Z.-x.; Liu, G.; Li, H.; Devereaux, T. P.; Yang, W. Cycling Mechanism of Li2MnO3: Li—CO2 Batteries and Commonality on Oxygen Redox in Cathode Materials. *Joule* **2021**, *5*, 975–997.
- (17) Haensel, R.; Keitel, G.; Sonntag, B.; Kunz, C.; Schreiber, P. Photoabsorption Measurement of Li, Be, Na, Mg, and Al in the XUV Range. *Phys. Status Solidi A* **1970**, *2*, 85–90.
- (18) Hightower, A.; Ahn, C. C.; Fultz, B.; Rez, P. Electron Energy-Loss Spectrometry on Lithiated Graphite. *Appl. Phys. Lett.* **2000**, 77, 238–240.
- (19) Schülke, W.; Nagasawa, H.; Mourikis, S.; Lanzki, P. Dynamic Structure of Electrons in Li Metal: Inelastic Synchrotron x-Ray Scattering Results and Interpretation beyond the Random-Phase Approximation. *Phys. Rev. B: Condens. Matter Mater. Phys.* **1986**, 33, 6744–6757.
- (20) Pascal, T. A.; Boesenberg, U.; Kostecki, R.; Richardson, T. J.; Weng, T.-C.; Sokaras, D.; Nordlund, D.; McDermott, E.; Moewes, A.; Cabana, J.; Prendergast, D. Finite Temperature Effects on the X-Ray Absorption Spectra of Lithium Compounds: First-Principles Interpretation of X-Ray Raman Measurements. J. Chem. Phys. 2014, 140, 034107.
- (21) Fister, T. T.; Schmidt, M.; Fenter, P.; Johnson, C. S.; Slater, M. D.; Chan, M. K. Y.; Shirley, E. L. Electronic Structure of Lithium Battery Interphase Compounds: Comparison between Inelastic x-Ray Scattering Measurements and Theory. *J. Chem. Phys.* **2011**, *135*, 224513.
- (22) Hohenberg, P.; Kohn, W. Inhomogeneous Electron Gas. *Phys. Rev.* **1964**, *136*, B864–B871.
- (23) Kohn, W.; Sham, L. J. Self-Consistent Equations Including Exchange and Correlation Effects. *Phys. Rev.* **1965**, *140*, A1133–A1138.
- (24) Shirley, E. L. Ab Initio Inclusion of Electron-Hole Attraction: Application to X-Ray Absorption and Resonant Inelastic X-Ray Scattering. *Phys. Rev. Lett.* **1998**, *80*, 794–797.
- (25) Rohlfing, M.; Louie, S. G. Electron-Hole Excitations and Optical Spectra from First Principles. *Phys. Rev. B: Condens. Matter Mater. Phys.* **2000**, *62*, 4927–4944.
- (26) Mauchamp, V.; Boucher, F.; Ouvrard, G.; Moreau, P. Ab Initio Simulation of the Electron Energy-Loss near-Edge Structures at the Li K Edge in Li, Li 2 O, and Li Mn 2 O 4. *Phys. Rev. B: Condens. Matter Mater. Phys.* **2006**, *74*, 115106.
- (27) Liang, Y.; Vinson, J.; Pemmaraju, S.; Drisdell, W. S.; Shirley, E. L.; Prendergast, D. Accurate X-Ray Spectral Predictions: An Advanced Self-Consistent-Field Approach Inspired by Many-Body Perturbation Theory. *Phys. Rev. Lett.* **2017**, *118*, 096402.

- (28) Liang, Y.; Prendergast, D. Quantum Many-Body Effects in x-Ray Spectra Efficiently Computed Using a Basic Graph Algorithm. *Phys. Rev. B* **2018**, *97*, 205127.
- (29) Liang, Y.; Prendergast, D. Taming Convergence in the Determinant Approach for X-Ray Excitation Spectra. *Phys. Rev. B* **2019**, *100*, 075121.
- (30) Yang, W.; Devereaux, T. P. Anionic and Cationic Redox and Interfaces in Batteries: Advances from Soft X-Ray Absorption Spectroscopy to Resonant Inelastic Scattering. *J. Power Sources* **2018**, 389, 188–197.
- (31) Li, Q.; Qiao, R.; Wray, L. A.; Chen, J.; Zhuo, Z.; Chen, Y.; Yan, S.; Pan, F.; Hussain, Z.; Yang, W. Quantitative Probe of the Transition Metal Redox in Battery Electrodes through Soft X-Ray Absorption Spectroscopy. *J. Phys. D: Appl. Phys.* **2016**, *49*, 413003.
- (32) Storr, J. NEXAFS Spectroscopy; Springer Series in Surface Sciences; Springer-Verlag Berlin Heidelberg, 1992; Vol. 25.
- (33) Yang, W. L. Band Structure and Fermi Surface of Electron-Doped C60 Monolayers. *Science* **2003**, *300*, 303–307.
- (34) Krisch, M. H.; Sette, F.; Masciovecchio, C.; Verbeni, R. Momentum Transfer Dependence of Inelastic X-Ray Scattering from the Li K Edge. *Phys. Rev. Lett.* **1997**, *78*, 2843–2846.
- (35) Zhuo, Z.; Pemmaraju, C. D.; Vinson, J.; Jia, C.; Moritz, B.; Lee, I.; Sallies, S.; Li, Q.; Wu, J.; Dai, K.; Chuang, Y.-d.; Hussain, Z.; Pan, F.; Devereaux, T. P.; Yang, W. Spectroscopic Signature of Oxidized Oxygen States in Peroxides. *J. Phys. Chem. Lett.* **2018**, *9*, 6378–6384.
- (36) Jiang, P.; Prendergast, D.; Borondics, F.; Porsgaard, S.; Giovanetti, L.; Pach, E.; Newberg, J.; Bluhm, H.; Besenbacher, F.; Salmeron, M. Experimental and Theoretical Investigation of the Electronic Structure of Cu 2 O and CuO Thin Films on Cu(110) Using x-Ray Photoelectron and Absorption Spectroscopy. *J. Chem. Phys.* 2013, 138, 024704.
- (37) England, A. H.; Duffin, A. M.; Schwartz, C. P.; Uejio, J. S.; Prendergast, D.; Saykally, R. J. On the Hydration and Hydrolysis of Carbon Dioxide. *Chem. Phys. Lett.* **2011**, *514*, 187–195.
- (38) Prendergast, D.; Galli, G. X-Ray Absorption Spectra of Water from First Principles Calculations. *Phys. Rev. Lett.* **2006**, *96*, 215502.
- (39) Mori-Sánchez, P.; Cohen, A. J.; Yang, W. Localization and Delocalization Errors in Density Functional Theory and Implications for Band-Gap Prediction. *Phys. Rev. Lett.* **2008**, *100*, 146401.
- (40) Perdew, J. P.; Yang, W.; Burke, K.; Yang, Z.; Gross, E. K. U.; Scheffler, M.; Scuseria, G. E.; Henderson, T. M.; Zhang, I. Y.; Ruzsinszky, A.; Peng, H.; Sun, J.; Trushin, E.; Görling, A. Understanding Band Gaps of Solids in Generalized Kohn–Sham Theory. *Proc. Natl. Acad. Sci. U.S.A.* **2017**, *114*, 2801–2806.
- (41) Perdew, J. P.; Burke, K.; Ernzerhof, M. Generalized Gradient Approximation Made Simple. *Phys. Rev. Lett.* **1996**, *77*, 3865–3868.
- (42) Heyd, J.; Scuseria, G. E.; Ernzerhof, M. Hybrid Functionals Based on a Screened Coulomb Potential. *J. Chem. Phys.* **2003**, *118*, 8207–8215.
- (43) Heyd, J.; Scuseria, G. E. Efficient Hybrid Density Functional Calculations in Solids: Assessment of the Heyd—Scuseria—Ernzerhof Screened Coulomb Hybrid Functional. *J. Chem. Phys.* **2004**, *121*, 1187—1192.
- (44) Janesko, B. G.; Henderson, T. M.; Scuseria, G. E. Screened Hybrid Density Functionals for Solid-State Chemistry and Physics. *Phys. Chem. Phys.* **2009**, *11*, 443–454.